Brain network similarity using k-cores

by

Kazi Tabassum Ferdous

A Thesis Submitted in Partial Fulfillment of the
Requirements for the Degree of

MASTER OF SCIENCE

in the Department of Computer Science

Brain network similarity using k-cores

by

Kazi Tabassum Ferdous

Supervisory Committee

Dr. Alex Thomo, Supervisor
(Department of Computer Science)

Dr. Venkatesh Srinivasan, Co-Supervisor
(Department of Computer Science)

ABSTRACT

Autism Spectrum Disorder (ASD) is extensively studied by medical practitioners, health researchers, and educators. ASD symptoms appear in early childhood, within the first two years of life, but diagnosing it remains challenging due to its complex and diverse nature. Nevertheless, early diagnosis is crucial for effective intervention. Traditional methods rely on behavioral observations, while modern approaches involve applying machine learning (ML) to brain networks derived from fMRI scans. Limited explainability of these advanced techniques poses a significant challenge in gaining clinician's trust.

This thesis builds on recent works that design explainable approaches for ASD diagnosis from fMRI data preprocessed as graphs. Our research makes three key contributions. Firstly, we demonstrate that a simple approach based on viewing graphs as tables and using tabular data classifiers can achieve the same performance as state-of-art, explainable graph theoretic methods. Secondly, we provide evidence that by adding higher-order connectivity information as attributes does not improve their performance. Most importantly, we show why the classification of brain networks is challenging by demonstrating the similarity between graphs belonging to individuals with ASD and those without, using a novel k-core based approach.

Contents

List of Tables

List of Figures

ACKNOWLEDGEMENTS

I would like to thank:

My husband (Mohammad Ali Akber) and my family, for encouraging me to pursue this degree and supporting me on this journey.

Dr. Alex Thomo, for providing me with this opportunity by hiring me as one of his research students and having faith in me.

Dr. Venkatesh Srinivasan, for mentoring, support, encouragement, and patience. I have learned a lot working with you.

Sowmya Balasubramanian for continuous supporting and encouragement throughout the research and writing this thesis.

There is no wrong decision in life as long as you can accept, adapt and make it work for you.

Anything you see in your mind, you can hold in your hands.

DEDICATION

Just hoping this is useful!

Chapter 1

Introduction

Autism Spectrum Disorder (ASD) is a developmental disorder caused by abnormal brain development, and encompasses a wide range of symptoms and severity levels, varying from mild to severe [16]. According to the Diagnostic and Statistical Manual of Mental Disorders (DSM-5) [4], a guide created by the American Psychiatric Association that health care providers use to diagnose mental disorders, people with ASD often have:

- Difficulty with communication and interaction with other people.
- Restricted interests and repetitive behaviors. Difficulties sharing in imaginative play or in making friends.
- Symptoms that affect their ability to function in school, work, and other areas of life
- Infrequently sharing interest, emotion, or enjoyment of objects or activities (including infrequent pointing at or showing things to others)
- Not responding or being slow to respond to one's name or to other verbal bids for attention. Having difficulties with the back and forth of conversation and without noticing that others are not interested or without giving others a chance to respond.
- Not displaying facial expressions, movements, and gestures and having an unusual tone of voice that may sound sing-song or flat and robot-like.

Autism is known as a "spectrum" disorder because there is wide variation in the type and severity of symptoms people experience. People of all genders, races, ethnicities, and economic backgrounds can be diagnosed with ASD. Although ASD can be a lifelong disorder, treatments and services can improve a person's symptoms and daily functioning. The exact cause of ASD is not fully understood, but research suggests that it results from a complex interplay of genetic and environmental factors [11, 15, 23, 32].

ASD Symptoms typically emerge in early childhood affecting approximately 1 in 36 children, with boys being diagnosed four times higher than girls. It occurs across different racial, ethnic, and socioeconomic backgrounds without specific limitations [9]. Although there is no cure for ASD, early intervention, specialized services, and parental support improve a child's growth and development [24].

Individuals with ASD may have co-occurring conditions such as Attention Deficit Hyperactivity Disorder (ADHD), anxiety, or depression, which need to be addressed for comprehensive support [18]. They also face challenges in social interactions, exhibit repetitive behaviors and often have heightened sensitivity (hypersensitivity) or reduced sensitivity (hyposensitivity) to stimuli like light, touch, taste, or smell [32].). ADHD is considered a chronic and debilitating disorder and is known to impact the individual in many aspects of their life including academic and professional achievements, interpersonal relationships, and daily functioning. An estimated 8.4% of children and 2.5% of adults have ADHD. Inattentive refers to challenges with staying and focusing on daily task, doesn't pay close attention or listen when spoken to. On the contrary, Hyperactivity refers to excessive movement such as fidgeting, excessive energy, not sitting still, and being talkative, interrupts or intrudes on other. There is a type of ADHD is diagnosed when both criteria for both inattentive and hyperactive/impulse types are met called "Combined Type". Despite this, they also possess remarkable strengths, such as visual thinking, strong visual and auditory learners and problem-solving abilities in math, science, music, or art.

Diagnosing ASD requires a comprehensive specialist evaluation [37] and a detailed clinical assessment based on specific criteria outlined in diagnostic manuals like the DSM-5 [4]. Nevertheless, this traditional diagnostic approach lacks definitive laboratory tests and relies heavily on clinical judgment and behavioral observations. Therefore, it is important to employ reliable methods to improve ASD diagnosis for all ages. Machine learning (ML) techniques have been shown to outperform humans in a variety of domains [7, 17, 19, 27].

The discovery of Functional MRI (fMRI), a modern brain imaging technique, has enabled researchers to identify and partition the brain into regions of interest (ROIs) based on their specific functions. By constructing a graph from fMRI scan, with ROIs as vertices and edges representing the co-activation of these regions, researchers can employ graph classification techniques to effectively classify fMRI scans [8]. Several techniques have been proposed for general graph classification such as kernel methods [45], graph embeddings [21], and deep learning [30]. Metrics such as accuracy, precision, and recall are essential for evaluating any such classifier [13], and it has been shown that some of these methods can achieve impressively high scores for the various metrics.

However, a drawback of these techniques is their complexity, large number of parameters, and black-box nature making it challenging to understand their predictions. Recently, there is a growing focus on *explainability* within the AI domain [22, 33]. In critical sectors like healthcare, decision-makers are hesitant to adopt prediction models solely based on the high reported accuracy without comprehending their decision-making processes [6]. This cautious approach is especially crucial in healthcare, where *explainability* is vital for gaining the trust of medical practitioners [48].

In response to the need for explainability, Lanciano *et al.* [31] used *contrast subgraph* method for diagnosing ASD. The goal is to find subgraphs in brain connectivity data that display dense connections among individuals with ASD while being sparse in neurotypical individuals, or vice versa. This approach aims to create an interpretable classification method revealing unique brain connectivity patterns in individuals with ASD. However, computing contrast subgraphs is complex and computationally intensive. In a recent study, Enns *et al.* [14] proposed a simpler *discriminative edges method*, which identifies the most important edges or connections that help distinguish individuals with ASD from neurotypical individuals. As shown in [14], both these methods obtained a mean accuracy of 60% on larger datasets of individuals with ASD. In light of these results, Enns *et al.* [14] poses the following question: Can brain imaging data lead to more accurate ASD diagnoses while maintaining explainability? If not, can we determine the reasons behind this limitation?

In our research, we seek to address this question by exploring an alternative pathway for explainable ASD diagnosis methods, complementing the findings of Lanciano *et al.* [31] and Enns *et al.* [14]. Our work views graphs as tables and focuses on demonstrating the effectiveness of simple and explainable tabular ML methods as alternatives to the graph techniques utilized in prior studies (e.g., [14,31]). Furthermore,

with the goal of improving the accuracy of our method, we explore the possibility of adding higher-order information as attributes to aid classification. While the methods we propose are simple and explainable, we observe that they did not achieve high accuracy though they matched the performance of the previous methods. Therefore, we investigate the potential barriers that hinder the achievement of strong performance metrics, aiming to provide insights into the question raised by [14]. Our main contributions are as follows:

1. Converting the brain network data into a tabular format and using explainable classifiers yield comparable results to graph-theoretic techniques used in prior works.

2. Incorporating higher-order connectivity patterns, the number of triangles in a node's neighbourhood, as attributes does not improve the classifier performance.

3. Studying similarities between brain networks of individuals with and without ASD, using similarity measures such as Jaccard similarity of k-cores and Hamming distance reveals the underlying barriers to ASD prediction.

The rest of the thesis is organised as follows:

Chapter 2 provides the essential contextual information required to comprehend the research conducted in this study, culminating in an exploration of relevant prior research.

Chapter 3 describes the data sets, approaches and methodologies to investigate the issues that were studied in this thesis.

Chapter 4 summarizes the conducted experiments within this study and analysis the outcomes obtained from these trials.

Chapter 5 states the conclusions of this study, answers the proposed research questions, and provides suggestions for future work.

Chapter 2

Related Work

The traditional approach involves utilizing behavioral and family history information for ASD diagnosis. Misman *et al.* [36] have claimed impressive accuracy rates up to 99% by employing Deep Neural Networks (DNNs) on ASD datasets that incorporate comprehensive behavioral and family history data. In an effort to improve the accessibility of these diagnosis techniques, Abbas *et al.* [1] developed mobile applications that coupled with machine learning techniques, show potential in aiding ASD diagnosis. However, it is important to note that relying solely on behavioral information may not provide an early and accurate diagnosis, as behavioral symptoms associated with ASD may not manifest until later in a child's development. Therefore, alternative methods focusing on biologically-based markers derived from fMRI scans are being explored.

Over the years, there has been extensive research on the classification of ASD [5, 29, 35, 40, 43, 50] using fMRI data. Several studies have explored diverse approaches to address this complex problem. The fact that the high accuracy is not unexpected stems from the current definition and diagnosis of ASD, which relies primarily on behavioral data. The primary aim of this research is to establish a dependable and informative method for ASD diagnosis that relies exclusively on biological markers detected in fMRI scans.

Machine learning approaches have been widely employed in ASD classification using fMRI data [34, 47]. Researchers have utilized correlation matrices and deep learning models to achieve accurate classifications. For example, Thomas et al. employed the collapsing of the temporal dimension using diverse metrics, including regional homogeneity. Following this data transformation, they inputted the resulting three-dimensional dataset into a 3D Convolutional Neural Network (3D-CNN). As a

result, their classification accuracies on the complete ABIDE datasets reached approximately 66%. Furthermore, they observed that utilizing an SVM classifier produced comparable outcomes [47].

Liu *et al.* [34] have used Extra Trees algorithm to select relevant features from correlation matrices derived from fMRI data, resulting in an accuracy of 72% on the ABIDE dataset. Deep Learning models, such as Dense Neural Networks (DNNs), have also shown promise in achieving high accuracy of 88%, often surpassing classical machine learning models [46].

Guo *et al.* employed sparse auto-encoders to extract features and then conducted a performance comparison of the deep neural network (DNN) when using these selected features versus utilizing the raw correlation values as inputs. The classifier that utilized the selected features achieved accuracy levels that were notably higher, with improvements of up to 9% [20]. In contrast to many other studies in this domain, which primarily concentrate on fine-tuning the architecture of their deep learning models, Guo's approach stands out by emphasizing feature engineering. This approach is distinct from those relying on complex feature selection methods that lack human interpretability [20, 29].

Feature selection techniques, such as sparse auto-encoders, have been employed to enhance classification performance and obtain accuracies above 90% [30]. Likewise, Iidaka utilizes effect-size thresholding to choose relevant features prior to applying a Probabilistic Neural Network (PNN) for classification. Their study focuses on a subset of the ABIDE dataset, specifically individuals under 20 years of age, and reports achieving an impressive accuracy rate of approximately 90% [25].

However, it is crucial to take into account the constraints associated with research conducted on small datasets, as such studies can lead to model overfitting and restrict their applicability to novel datasets. Continual research is being conducted to achieve strike a balance between model performance and interpretability, as deep learning models are often considered "black-box" classifiers. Efforts are being made to develop explainable classification methods [22,33,51], allowing researchers and neuroscientists to gain insights and trust the predictions made by these models. These methods, such as [41], often involve deriving explanations for the model's decisions, such as SHAP values. Abrate and Bonchi devised an approach aimed at discovering counterfactual graphs in order to elucidate the functioning of black-box classifiers. However, this method comes with a high computational cost and exclusively mirrors the elements the classifier considers significant, without necessarily guaranteeing the

practical relevance of this information for accurate classification [2]..

The present study is inspired by the work of Lanciano *et al.* [31]. They prioritized interpretable and simple features to aid neuroscientists' understanding, rather than solely aiming for high accuracy. In a similar vein, Coupette *et al.* [10] developed an algorithm to identify characteristic subgraphs with common and contrasting structures in graph groups, and illustrated their technique using brain networks from adolescents in the ABIDE dataset. Wang and colleagues recently introduced an innovative approach for universally embedding entire graphs without the need for hyperparameters, referred to as DHC-E (Degree, H-index, and Coreness theorem along with Shannon Entropy). This embedding method yields a moderate number of dimensions, contingent on the specific graph dataset under consideration, and is constructed using the h-index values associated with each vertex within the graph [49].

Finally, Enns *et al.* [14] proposed the discriminative edges method with the goal of identifying a set of important edges that can separate the two classes. All these studies aim to uncover meaningful patterns in brain networks to enhance our understanding of ASD.

Chapter 3

Datasets and Methods

In this section, we will first describe the datasets we use and the preprocessing steps involved in generating brain networks. Then, we will outline the methodologies employed for the classification and comparison of these brain networks.

3.1 Dataset Description

The study described in Section 4.1 utilizes the dataset obtained from Lanciano *et al.* [31] (`https://github.com/tlancian/contrast-subgraph`), which was originally released by the Autism Brain Imaging Data Exchange (ABIDE) project [3]. TAutism Brain Imaging Data Exchange (ABIDE) initiative has aggregated functional and structural brain imaging data collected from laboratories around the world to accelerate our understanding of the neural bases of autism. In August 2012, the Autism Brain Imaging Data Exchange (ABIDE) released data for their first initiative known as ABIDE I referred to simply as the ABIDE data set from here on [12]. ABIDE now includes two large-scale data collections ABIDE I and ABIDE II. Each collection is an aggregation of datasets collected from 24 international brain imaging laboratories and is made available to researchers and investigators to understand and reveal the brain mechanisms underlying ASD.

ASD Dataset

The ASD dataset consists of neuroimaging data from 1112 individuals, comprising 573 Typically Developed (TD) individuals and 539 individuals diagnosed with Autism Spectrum Disorder (ASD). Typically Developed (TD) individuals have normal brain

function without neurological disorders whereas Autism Spectrum Disorder (ASD) individuals face autism-related challenges. The dataset also includes phenotypic data about the individuals with information such as each subject's age, sex, and whether the subject's eyes were closed during the scan. Each individual in the dataset is represented by an undirected unweighted graph containing 116 vertices, where each vertex corresponds to a Region of Interest (ROI). The presence of an edge in the graph indicates strong a correlation in the activity between the two ROIs. The graphs are represented by an adjacency matrix of size 116×116.

Lanciano *et al.* created four distinct datasets from the original ABIDE source [3]. These datasets were curated by selecting individuals based on shared characteristics, such as age, gender, and scan conditions (e.g., eyes closed or male), as shown in Table 3.1. Each of the hdataset are divided into two classes namely TD and ASD and the dataset's description reflects shared phenotypic features among the observations. For instance, the "Children" dataset comprises individuals aged 9 years or younger, the "Adolescents" dataset includes individuals aged between 15 and 20 years, the "EyesClosed" dataset consists of individuals who underwent fMRI scans with their eyes closed, and the "Male" dataset exclusively includes male individuals.

Dataset	**Description**	**TD**	**ASD**
Children	Age ≤ 9	52	49
Adolescents	Age in [15,20]	121	116
EyesClosed	During scanning eyes are closed	158	136
Male	Male individuals	418	420

Table 3.1: ASD Dataset - Lanciano *et al.*

ADHD Dataset

In our experiments, as described in Section 4.2, we also used an ADHD dataset, which is another neurodevelopmental disorder impacting individuals of various age groups. ADHD is characterized by attention difficulties and impulsivity. Like ASD, the exact causes of ADHD remain unclear, and there is presently no cure for either condition. Nevertheless, treatments such as behavioral therapy and medication aid in symptom management and improving daily functioning [38]. By incorporating the ADHD dataset into our experiments, we gain valuable insights into the applicability of our techniques and results for ASD to other related disorders like ADHD.

Dataset	Description	TD	ADHD
ALL	ALL	330	190

Table 3.2: ADHD Dataset - Abrate *et al.*

This study uses the ADHD dataset from [2] (`https://github.com/carlo-abrate/CounterfactualGraphs`) which includes 330 individuals with typical development (TD) (normal brain function) and 190 individuals diagnosed with ADHD, as summarized in Table 3.2. Similarly to the ASD dataset in Section 3.1, the ADHD dataset also portrays each individual with an undirected unweighted graph of 190 vertices, representing regions of interest (ROIs). The presence of an edge in the graph signifies a substantial correlation in the activity between the two ROIs, resulting in a adjacency matrix of size of 190×190.

For the parcellation of the brain the authors of [31] used the AAL atlas for the ASD dataset ($|V| = 116$) and the authors of [2] used Craddock 200 (CC200) for the ADHD dataset $|V| = 190$).

3.2 Data Preprocessing

In our work, we use the ASD and ADHD graph datasets as provided by the authors of [2,31], without requiring any additional preprocessing. However, for completeness, we briefly outline the preprocessing steps needed to convert fMRI scans into graphs. The advancement of magnetic resonance imaging (MRI) methods has opened up opportunities in the field of connectomics which explores structural and functional connections between neurons in the brain and nervous system. It represents the brain as a network which facilitates the investigation of captivating neuroscience research questions using graph analysis methodologies. A connectome refers to a comprehensive map that describes the neural connections between specific regions of interest (ROIs) within the brain. This mapping can be achieved through two approaches: Structural and Functional connectome. By analyzing fMRI scans of individuals affected by a mental disorder in comparison to scans of healthy individuals, the objective is to uncover patterns within their respective connectomes. These patterns aim to elucidate the distinctions in brain mechanisms between the two groups. The identification of such patterns holds significant potential for gaining valuable insights into the disorder and suggesting strategies to enhance the well-being of patients.

Resting state fMRI is a neuroimaging technique that works by measuring the blood-oxygen-level-dependent (BOLD) signals in the brain. When a region of the brain becomes active, there is an increased demand for oxygenated blood to support the active neurons in that region. Therefore, the body responds by increasing the flow of oxygenated blood to that region. fMRI takes advantage of this body response to measure brain activity indirectly via BOLD signal intensities in different regions. The choice of the size of each region, and hence the number of such regions, is done using a brain atlas (AAL atlas, CC200). These regions are referred to as regions of interest (ROI). The temporal resolution (TR) in scanning refers to the time interval between consecutive samples taken from a subject's brain. Typically, this interval is a few seconds, but it may vary depending on the specific research study [30].

For each scan of the subject's brain, a three-dimensional image representing BOLD signal intensities is generated. Multiple scans of the brain are conducted during a session, producing a collection of three-dimensional images that illustrate how the BOLD signal in the brain changes over time. The BOLD signal measurements' level of detail is established by voxels, which are three-dimensional pixels typically on the order of cubic millimeters in size. These voxels each represent a time series, recording BOLD intensity values throughout the fMRI scans, and can be aggregated to form Regions of Interest (ROIs) within the brain. The assembly and identification of these voxels into ROIs are facilitated by the utilization of a brain atlas.

In Figure 3.1, we can observe the time series data for three Regions of Interest (ROIs) within the brain of a single subject. These ROIs exhibit fluctuations in their BOLD signals throughout the scan. It's evident that there is a strong correlation between the blue and orange time series, while there is a notable lack of correlation between both the blue and orange time series and the green time series. It is widely accepted that functional connections between ROIs can be inferred from the degree of correlation in their BOLD time series [2]. When two regions consistently display similar BOLD signal activity, they are considered to be functionally connected. The determination of the correlation between two sets of data points is frequently computed using the Pearson correlation coefficient.

In summary, the output of an fMRI scan is a 3-dimensional image of the BOLD signal intensities in different ROIs of the brain measured over time. The process of transforming BOLD time series for each Region of Interest (ROI) into graph data involves following essential steps:

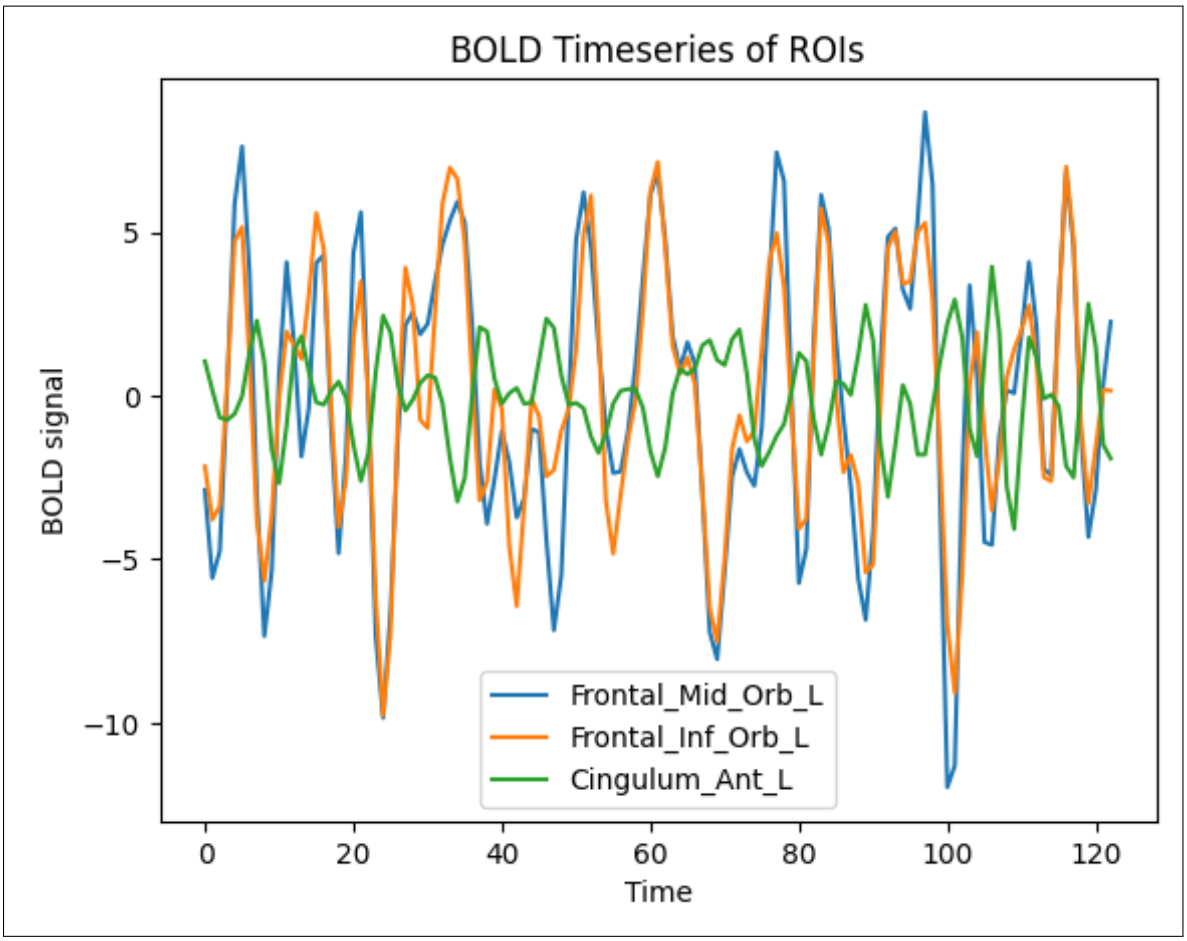

Figure 3.1: BOLD time series of three ROIs from the ABIDE dataset. The ROIs are labelled according to the AAL label file provided by the PCP. The orbital region of the left middle frontal gyrus and the orbital region of the left inferior frontal gyrus are highly correlated, whereas the left anterior cingulate and paracingulate region is negatively correlated to the others .

1. **Time Series Extraction:** The communication pattern between two brain regions is examined by comparing their BOLD time series. The underlying premise is that the level of functional connections between two regions can be determined by assessing the correlation in their BOLD time series. The higher the correlation, the higher the functional connectedness.

2. **Calculate Pearson correlation coefficients (PCC):** After completing the previous step, we obtain a dataset for a single patient, comprising 116 time series, each corresponding to a Region of Interest (ROI). Each of these time

series has a length of 145 data points. Pairwise PCC is calculated between the BOLD time series for every pair of ROIs. This step yields a correlation matrix of size 116 × 116 (for ASD) or 190 × 190 (for ADHD), containing values in the range [-1, +1]. The correlation matrix acts as a weighted adjacency matrix, with ROIs as nodes and correlation coefficients as edge weights.

3. **Apply threshold:** Thresholding retains only the strongest connections and its value is established to be equal to the 80th percentile of the distribution of correlation values. Subsequently, we establish an edge between each pair (u,v) of ROIs if their correlation value exceeds this threshold.

4. **Graph Construction:** The significant connections are represented as edges or links between the ROIs, and the ROIs themselves are represented as nodes. The outcome of this procedure is the creation of an undirected and unweighted graph, similar to what is done with the ASD and ADHD datasets. This involves using the connectivity matrix and the thresholded correlation matrix to construct the graphical representation of the data.

5. **Graph Analysis:** Various graph analysis techniques can be applied to explore the characteristics of the brain connectivity graph. These techniques include measures such as network density, clustering coefficient, modularity, path length, and centrality measures (e.g., degree centrality, betweenness centrality). These measures provide insights into the organization, efficiency, and integration of the brain network.

6. **Visualization:** The graph can be visualized using network visualization tools, such as Gephi, Cytoscape, or BrainNet Viewer. Visualization helps in interpreting and communicating the complex connectivity patterns in a more intuitive manner.

   By converting fMRI data into graphs, researchers can examine the connectivity patterns and network properties of the brain. Graph-based analyses facilitate

the understanding of functional relationships between different brain regions and help uncover alterations in connectivity associated with various neurological and psychiatric conditions, including Autism Spectrum Disorder (ASD)

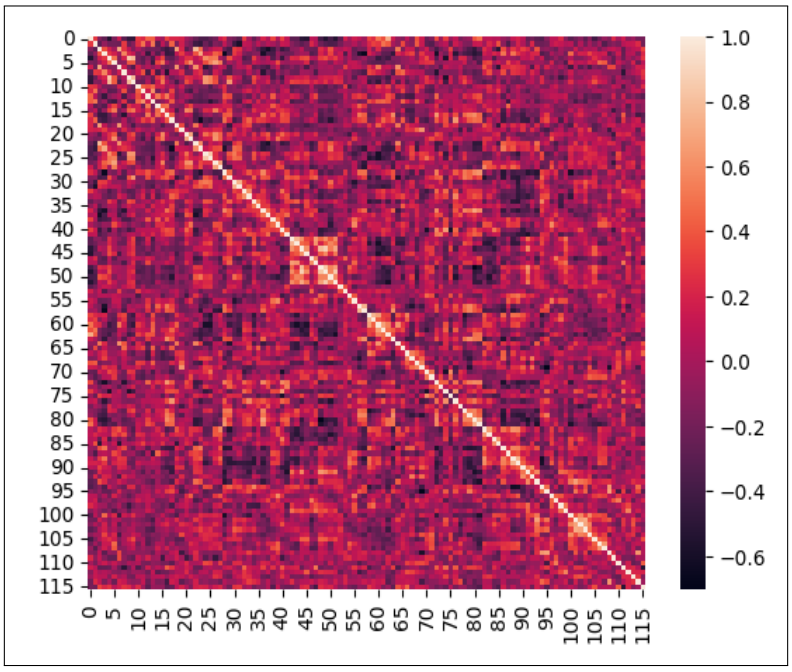

Figure 3.2: The correlation matrix of the subject in Figure 3.1. The blue circle indicates the high correlation value between the correlated ROIs, whereas the green circles indicate the negative correlation values between the third ROI and the others. The matrix represents the pairwise Pearson correlation coefficients of every ROI in the brain. The matrix is symmetric, and the main diagonal contains zeros as the correlation of each ROI to itself is irrelevant.

Figure 3.2 illustrates a correlation matrix generated through pairwise calculations for a single subject. It's important to conceptualize this correlation matrix as the weighted adjacency matrix of a brain network. In other words, the Regions of Interest (ROIs) in the brain can be regarded as the nodes of this brain network or graph, and the correlation coefficients signify the edges within the network. This perspective is fundamental when considering and interpreting these correlation matrices in subsequent analyses.

3.3 Classification Methods of Brain Networks

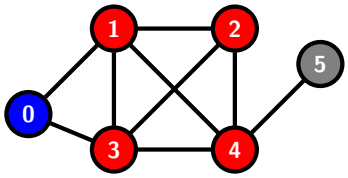

(a) Graph $\mathcal{G}$

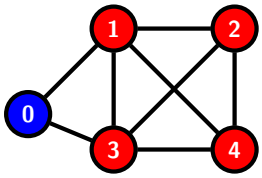

(b) 2-core of $\mathcal{G}$

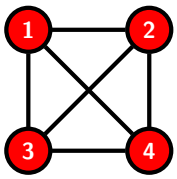

(c) 3-Core of $\mathcal{G}$

Figure 3.3: Different Core of Graph $\mathcal{G}$

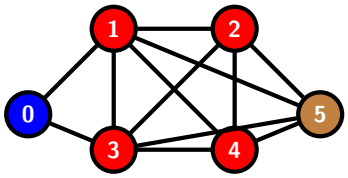

(a) Graph $\mathcal{G}'$

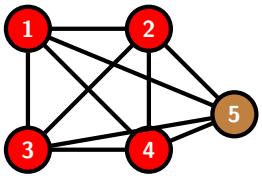

(b) 4-core of $\mathcal{G}'$

Figure 3.4: Different Core of Graph $\mathcal{G}'$

Graphs as tables. The graph can be represented as matrix and the size of the matrix is total number of vertices by the total number of vertices. Here, rows and columns both represent vertices, and its filled with either 1 or 0. Recall that brain networks are represented as an undirected graph on 116 vertices in which each vertex has a unique id between 1 and 116. In order to convert a collection of such vertex-labeled brain networks into a table, we create a table with $\binom{116}{2} = 6670$ columns so that the table has one column for each possible edge in the graph. We can then represent any brain network G as a binary vector, $T(G)$, of length 6670 such that a bit location labeled by i & j stores a 1 if the edge is present in G and 0 otherwise. We assume that the edges are listed in the lexicographic order.

Example. For the graph G shown in Fig. 3.3(a), the binary vector corresponding to G, $T(G)$, is [101001110110101].

Example. For the graph G' shown in Fig. 3.4(a), the binary vector corresponding to G', $T(G')$, is [101001111111111].

Tabular Classifiers. Tabular classifiers" typically refer to machine learning or statistical classifiers that operate on structured data presented in a tabular format, often with rows and columns. Transforming graph data into tables enables organized and structured analysis. Tabular classifiers are commonly used for tasks such as classification, regression, and pattern recognition. Tables provide a tabular representation that allows for easier data manipulation, sorting, filtering, and statistical analysis compared to the graphical representation of the graph data. These classifiers can include various algorithms depending on the specific problem and dataset. Different algorithms may perform better or worse depending on the data's characteristics. In this study, we utilize various tabular classifiers, including *SVM, Linear Regression, k-nearest neighbors (KNN), XGBoost, AdaBoost, and Perceptrons.* We evaluate performance using the four metrics: *Accuracy, Precision, Recall, and F1-score.* While all metrics are important, we present the top-3 classifiers selected based on their *accuracy* in Section 4. Our emphasis on accuracy aligns with previous works [14, 31].

Local Clustering Coefficient. Informally, the local clustering coefficient of a node i, denoted as C_i, in a graph quantifies the probability or likelihood that the neighbors of node i are also directly connected to each other. In simpler terms, it assesses how tightly-knit or clustered the immediate network surrounding node i is. A high local clustering coefficient suggests that the neighbors of i are well-connected, while a low coefficient indicates that they are less likely to be connected to each other. This term was coined by Watts and Strogatz in 1998. Formally,

$$C_i = \frac{|\{(j,k) \mid j,k \in N_i, (j,k) \in E\}|}{\binom{|N_i|}{2}}$$

where N_i is the set of neighbours of node i. For each brain network, we will compute a tuple of size 116 containing the local clustering coefficient of its vertices.

Example. For the graph $\mathcal{G}$ in Fig. 3.3(a), the local clustering coefficient of vertex 0 is $C_0 = \frac{1}{\binom{2}{2}} = 1$ while $C_1 = \frac{4}{\binom{4}{2}} = 2/3$.

Example. For the graph $\mathcal{G}'$ in Fig. 3.4(a), the local clustering coefficient of vertex 0 is 1 while $C_1 = \frac{7}{\binom{5}{2}} = 7/10$.

The local clustering coefficient is a measure introduced by Watts and Strogatz to study small world theory in social networks. As it measures interconnectedness

among neighbors by counting triangles (a small graph pattern) centered at a node in essence, adding it as an additional attribute provides extra information about the graph and helps with ML tasks.

Top 5 Nodes. The analysis of the top 5 nodes in a graph involves identifying the nodes that are most central or influential within the network based on their participation in triangles or other specific structural patterns. These nodes play a crucial role in understanding the network's characteristics and can have implications in various fields, including social network analysis, biological network analysis, and more. One common approach is to measure the number of triangles each node participates in.

A triangle consists of three nodes connected to each other. Nodes that participate in many triangles are considered important because they connect multiple parts of the network.

Let $G = (V, E)$ be a graph, where V represents the set of nodes (vertices) and E represents the set of edges.

For each node $v_i \in V$, count how many triangles it participates in. This can be represented as $C(v_i)$, which is the count of triangles containing node v_i.

Nodes are ranked based on their triangle participation counts in descending order. Nodes ranked list is created of nodes with the highest $C(v_i)$ values at the top. Let's denote this ranking as R. Then, the top 5 nodes are selected from the ranked list R. These nodes will be the top 5 nodes in the graph in terms of their involvement in triangles.

In summary, the analysis of the top 5 nodes in a graph is a valuable technique for understanding network structure and identifying influential elements. However, it should be complemented with other centrality measures and domain-specific knowledge to obtain a comprehensive view of network dynamics and node importance.

3.4 Comparison Methods of Brain Networks

Comparing brain networks is a crucial task in neuroimaging and network neuroscience, as it helps researchers gain insights into the structure and function of the brain. The choice of method such as Machine Learning and Classification, Graph Metrics Comparison or Edge-Wise Comparison depends on the research question, data availability, and the specific aspects of brain networks. Researchers often employ a combination of these methods to gain a comprehensive understanding of brain network differences

and similarities in various contexts. We use different methods to compare the collection of brain networks belonging to the two classes, ASD and TD: Hamming distance, k-core decomposition and Jaccard Similarity.

Hamming Distance. Hamming distance is typically used to measure the difference between two strings or binary vectors of equal length. However, in certain contexts, this concept of Hamming distance can be adapted as metric for measuring the difference between graphs. Given two graphs $\mathcal{G}$ and $\mathcal{G}'$ on n vertices, the Hamming distance between graph $\mathcal{G}$ and $\mathcal{G}'$ is the minimum number of edge insertions and deletions needed to convert graph $\mathcal{G}$ to $\mathcal{G}'$. Equivalently, the Hamming distance between graph $\mathcal{G}$ and $\mathcal{G}'$ is the number of bit positions in which the two binary strings $T(\mathcal{G})$ and $T(\mathcal{G}')$ differ.

Example. Consider $\mathcal{G}$ and $\mathcal{G}'$ in Fig.3.3(a) and Fig.3.4(a). We need to add edges $(1, 5)$, $(2, 5)$ and $(3, 5)$ to convert $\mathcal{G}$ to $\mathcal{G}'$. Hence, the Hamming distance is 3.

k-Core of a Graph G. The k-Core of a graph is a maximal subgraph in which every vertex has at least degree k. k-Cores are used to identify the most tightly connected parts of a graph and can provide insights into the overall structure and behavior of a network. For a graph G on n vertices and an integer k, $1 \leq k \leq n$, the k-core of G is the maximal subgraph H of G such that the induced degree of every vertex in H is at least k.

Note that, by the above definition, the $k + 1$-core of G is a subset of the k-core of G, and hence the set of k-cores, $1 \leq k \leq n$, as k increases from 1 to n form a nested structure. This nested structure is referred to as k-core decomposition in the literature [28].

Example. Fig. 3.3(b) is the 2-core of the graph $\mathcal{G}$ in Fig. 3.3(a). In Fig. 3.3(b), each vertex is connected to at least 2 other vertices and it is also the maximal subgraph with that property. Note that 1-core of $\mathcal{G}$ is $\mathcal{G}$.

Fig. 3.4(b) is the 4-core of the graph $\mathcal{G}'$ in Fig. 3.4(a). In Fig. 3.4(b), each vertex is connected to at least 4 other vertices and it is also the maximal subgraph with that property. Note that 2-core of $\mathcal{G}'$ is $\mathcal{G}'$.

k-core decomposition is often used in graph analysis and network science to identify important substructures within a network. The k-core can help reveal the central and densely connected regions of a graph, which can be useful in various applications, such as identifying communities or detecting important nodes in complex networks.

Max-Core of a Graph G. The maximum core (Max-Core) of a graph G is the highest possible value of k for which G contains a k-core. A k-core in a graph is a subgraph in which all vertices have a degree of at least k. In other words, it's the largest subgraph where each vertex has at least k neighbors within that subgraph.

The process of finding the Max-Core involves iteratively identifying and removing vertices with degrees less than k until no such vertices exist while keeping track of the current value of k. This process continues until no core greater than the current k is found.

In summary, the Max-Core of a graph represents the maximum size of a k-core that can be extracted from the graph by iteratively removing low-degree vertices.

Example. Fig. 3.3(c) is the 3-core of graph $\mathcal{G}$ in Fig. 3.3(a). In Fig. 3.3(c), each vertex is connected to at least 3 other vertices and it is also the max-core as the 4-core of $\mathcal{G}$ is empty.

Fig. 3.4(b) is the 4-core of graph $\mathcal{G}'$ in Fig. 3.4(a). In Fig. 3.4(b), each vertex is connected to at least 4 other vertices and it is also the max-core as the 5-core of $\mathcal{G}'$ is empty.

To compare max-cores of two different graphs G_1 and G_2, we will use the notion of Jaccard similarity. Let V_1 and V_2 denote the set of vertices of G_1 and G_2. We use this property to understand the similarity two graphs G_1 and G_2 based on vertices.

Jaccard Similarity. Jaccard similarity is a metric used to measure the similarity between two sets. It is particularly useful when you want to compare the similarity between sets of elements without considering their order. Jaccard similarity is defined as the size of the intersection of the sets divided by the size of their union. Given two sets V_1 and V_2, we define their Jaccard similarity, $JS(V_1, V_2)$ as:

$$JS(V_1, V_2) = \frac{|V_1 \cap V_2|}{|V_1 \cup V_2|}$$

Example. Fig. 3.3(c) is the max-core G_1 of graph G and has vertices $V_1 = \{1, 2, 3, 4\}$. Lets assume G_2 is the max-core of another graph and has vertices $V_2 = \{1, 2, 7, 8, 9\}$, Jaccard similarity is computed as: $JS(V_1, V_2) = \frac{2}{7}$.

Fig. 3.4(b) is the max-core G_1' of graph G' and has vertices $V_1 = \{1, 2, 3, 4, 5\}$. Lets assume G_2' is the max-core of another graph and has vertices $V_2 = \{2, 5, 7, 8, 9\}$, Jaccard similarity is computed as: $JS(V_1, V_2) = \frac{2}{8} = \frac{1}{4}$.

Chapter 4

Results and Discussion

This chapter will provide a concise overview of the experiments conducted in this study, including any paths that were deemed infeasible. Subsequently, it will present the results obtained from these experiments. It's important to highlight that the entire progression of the experimentation phase can be monitored by reviewing the Git history of this thesis's repository, which is accessible in the Appendix A

4.1 Insights on ASD Dataset

The objective of this experiment is to enhance the accuracy of brain classification. There exist various approaches for classifying brain data, with one straightforward alternative being the transformation of a graph into a table. The first research question of this study to investigate the potential of achieving interpretability through tabular classification.

RQ1: How do well-known tabular classifiers perform on brain networks in tabular format?

By converting the graph dataset into tabular form, as described in Section 3, we can employ a wide array of well-known tabular classifiers for flattened brain networks. Figure 4.1 presents our results (using ten-fold cross-validation), showing SVM (with a linear kernel) and Linear Regression (LR) consistently ranking among the top-3 classifiers across all four ASD datasets. These classifiers achieve a mean accuracy of close to 60% on larger datasets, like Male. The balanced nature of the ASD datasets sets the baseline accuracy at 50%.

Enns *et al.* aimed to replicate Lanciano *et al.* work to comprehend the reported

high accuracy. However, their results differed from the original study, demonstrating mean accuracies of 73.5% for Children, 60.8% for Adolescents, 58.5% for EyesClosed, and 59.3% for Male on the ASD dataset (Enns *et al.*, Table 4.2 in [14]). Our RQ1 results demonstrates a simple, alternate strategy to achieve explainability in ASD diagnosis using brain networks.

The main observation here is the strong performance of SVM and LR classifiers, particularly on the larger datasets, indicating their potential significance in ASD diagnosis. Interestingly, these two classifiers boast high explainability, and their accuracy closely matches that of the more sophisticated graph-theoretic methods from previous studies ([14, 31]) known for their explainable nature. This finding underscores the relevance and competitiveness of SVM and LR classifiers in the context of ASD diagnosis, even compared to more complex graph-based techniques. Enns *et al.* aimed to replicate Lanciano *et al.* work to comprehend the reported high accuracy. Enns *et al.* (Table 4.2 in [14]) showed that the contrast subgraph method achieved mean accuracies of 73.5% for Children, 60.8% for Adolescents, 58.5% for EyesClosed, and 59.3% for Male on the ASD dataset. Our results for RQ1 demonstrate a simple, alternate strategy to achieve explainability for ASD diagnosis using brain networks.

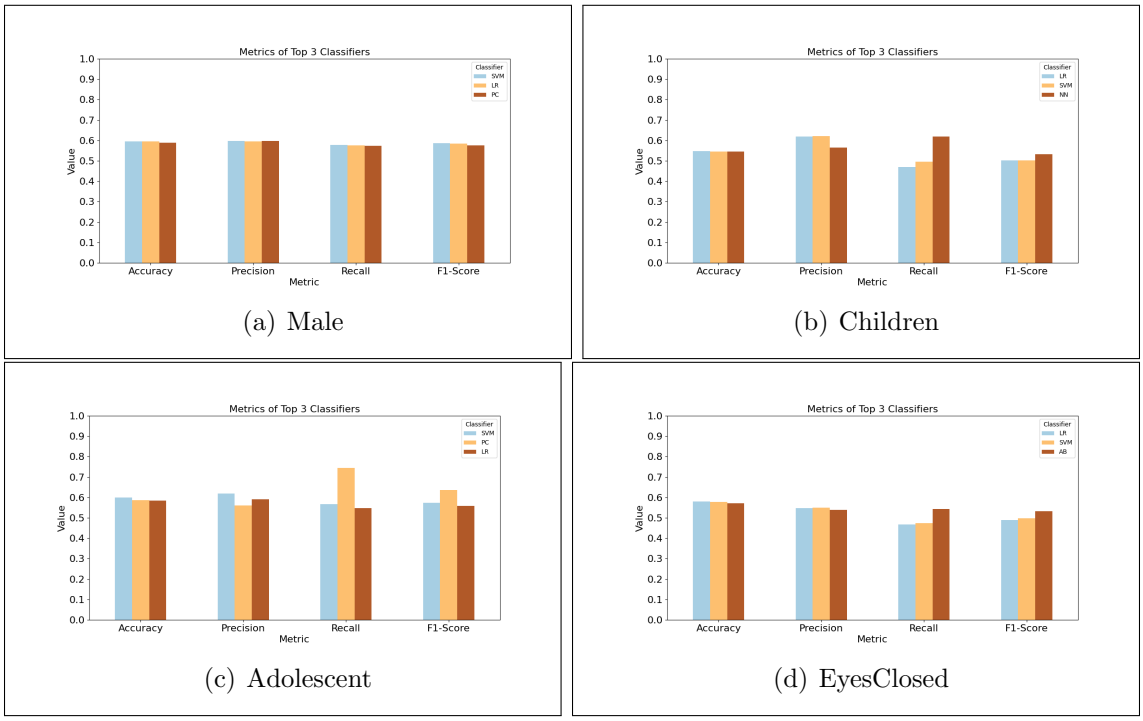

(a) Male

(b) Children

(c) Adolescent

(d) EyesClosed

Figure 4.1: RQ1 - Performance Metrics of Top-3 Classfiers

Dataset	**Class(Accuracy)**		
Male	SVM(0.59)	LR(0.58)	Pc(0.58)
Children	SVM(0.54)	NN(0.54)	LR(0.54)
Adolescent	SVM(0.60)	KNN(0.58)	LR(0.58)
Eyesclosed	LR(0.58)	SVM(0.57)	AB(0.57)

Table 4.1: RQ1- Performance Metrics Table of Top-3 Classifiers

Our second question stems from the knowledge that graph classifiers can benefit from additional attributes beyond node and edge information as shown in [42].

RQ2: Can incorporating higher-order connectivity patterns, such as triangles, as attributes improve the performance of tabular classifiers?

From the previous inquiry, we have established that the inclusion of higher-order connectivity patterns is poised to enhance accuracy. Higher-order connectivity entails the examination and quantification of connections or relationships that extend beyond traditional pairwise edges. This approach delves into more intricate graph patterns, facilitating the identification of multi-node pathways, subsets of nodes where each node connects with every other, densely interlinked nodes within a graph, and recurring subgraph patterns (motifs) embedded within the larger graph structure. On the whole, the analysis of higher-order connectivity provides a more comprehensive and nuanced grasp of intricate systems and networks. It serves as a valuable tool for uncovering concealed structures, refining predictive models, and making well-informed decisions across diverse domains. In light of this rationale, we will employ the clustering coefficient and examine the top 5 nodes within triangle patterns to address RQ2.

Clustering Coefficient Analysis: Our initial investigation focuses solely on the clustering coefficient information to assess potential enhancements in performance metrics, utilizing a ten-fold cross-validation approach. To facilitate this objective, we have curated a tabular dataset, where each row corresponds to a brain network, featuring 116 columns dedicated to storing the local clustering coefficients of the network's nodes. In Table 4.2, we present the accuracy results for the top three performing classifiers (SVM, LR, NN) in the male dataset, achieving an accuracy rate of 55%. In the case of the children's dataset, the highest accuracy obtained is 62%, while for the eyesclosed dataset, the peak accuracy reaches 53% with the decision tree classifier. Lastly, in the Adolescent dataset, the k-nearest neighbor algorithm yields the highest accuracy, reaching 56%. It is evident that the Decision Tree algorithm outperforms other algorithms in terms of accuracy for two datasets, achieving the highest accuracy of 62% on the children dataset.

Dataset	**Class(Accuracy)**		
Male	SVM(0.55)	NN(0.54)	LR(0.54)
Children	DT(0.62)	NB(0.57)	AB(0.56)
Adolescent	KNN(0.56)	DT(0.52)	AB(0.50)
Eyesclosed	DT(0.53)	SVM(0.62)	AB(0.51)

Table 4.2: RQ2 - Clustering Co.for ASD Dataset

Top 5 Node Analysis: In the second phase of our study, we will focus on utilizing the top 5 nodes and evaluate the accuracy for each dataset. This involves identifying nodes within a graph that participate in the highest number of triangles, ranking them in descending order based on their triangle participation counts. To facilitate this analysis, we've compiled a tabular dataset where each row corresponds to a brain network, featuring 5 columns dedicated to storing the top 5 node numbers of the brain network. In Table 4.3, we present the accuracy results for the top performing classifiers are SVM, AB and KNN in the male dataset, achieving an accuracy rate of 53%. For children dataset top performing classifier is AB with 56% accuracy. Eyesclosed dataset highest accuracy is 56% for SVM and Adolescents dataset highest accuracy is 53% for Decision Tree. Among the various algorithms analyzed for the top 5 nodes, SVM stands out with the highest accuracy of 56%, surpassing the performance of other methods.

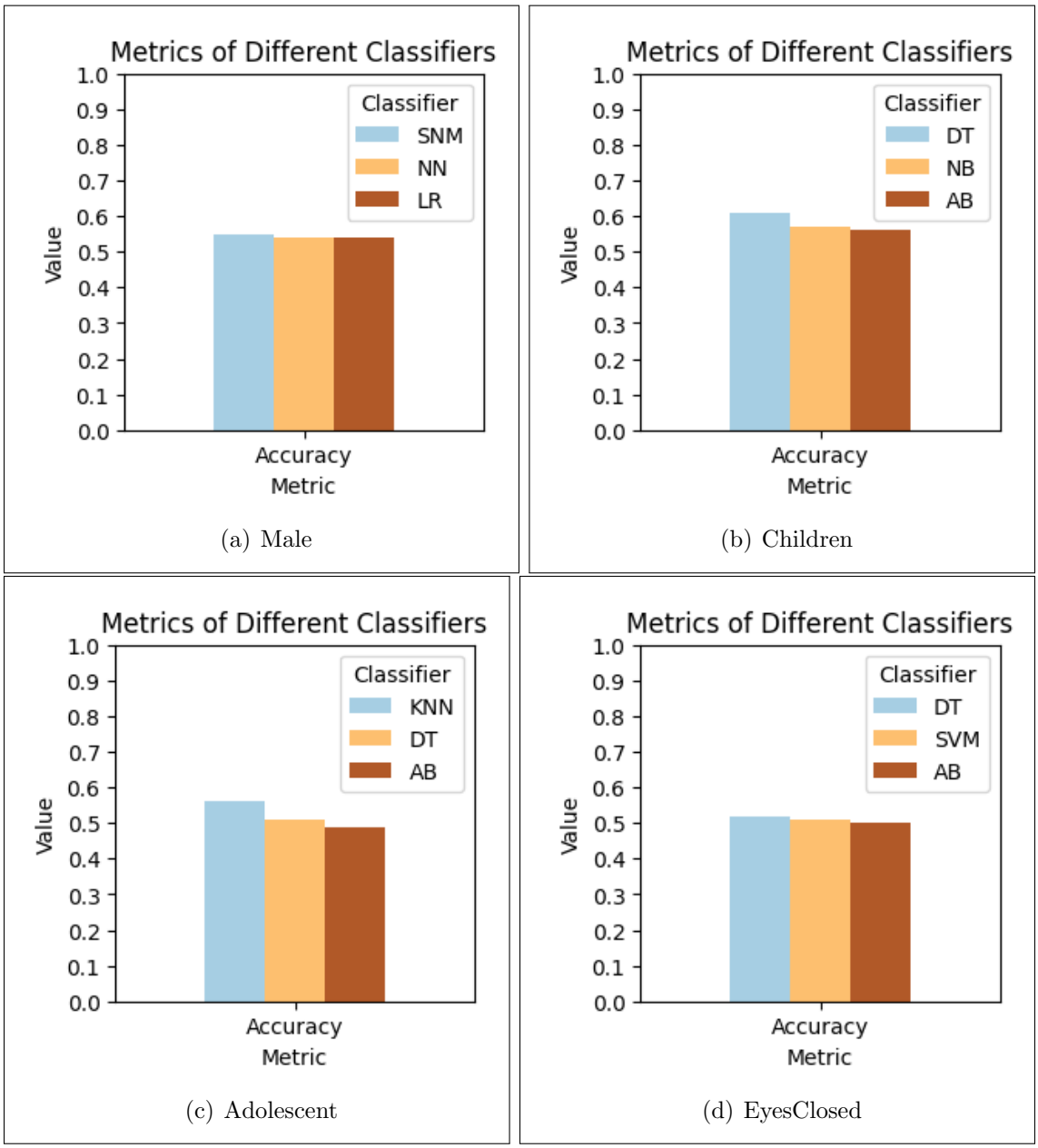

(a) Male (b) Children

(c) Adolescent (d) EyesClosed

Figure 4.2: RQ2 - Performance Metrics of Top-3 Classfiers for Clustering Co.

As we have observed the accuracy for individual higher-order connectivity patterns, it is worth noting that by combining these higher-order connectivity patterns with augmented tables, we introduce additional information that is expected to enhance the classifier's performance.

Dataset	**Class(Accuracy)**		
Male	SVM(0.53)	AB(0.53)	KNN(0.51)
Children	AB(0.56)	XG Boost(0.55)	NB(0.51)
Adolescent	DT(0.53)	XG Boost(0.52)	NN(0.52)
Eyesclosed	SVM(0.56)	LR(0.54)	XG Boost(0.52)

Table 4.3: RQ2 - Top 5 Nodes for ASD Dataset

Augmented Table Analysis: To address Research Question 1 (RQ1), we initially converted the graph dataset into tabular form. Subsequently, we expanded this table by incorporating new attributes, specifically the local clustering coefficients and the top 5 nodes. With this augmented table in hand, we proceeded to train tabular classifiers using a ten-fold cross-validation approach. However, the outcome of our analysis suggests that there is no significant enhancement in the performance metrics despite the inclusion of these additional attributes. Table 4.4 displays the top three classifiers results in this scenario. Male and Eyesclosed datasets has accuracy of 60% and 62% respectively for SVM. The accuracy for the Children dataset is 56% for AB, but it notably acquired accuracy to 62% when only considering clustering coefficient information has been used. For Adolescent dataset accuracy is 59% for LR.

Figure 4.4 presents our results (using ten-fold cross-validation), showing SVM (with a linear kernel) consistently ranking among the top-3 classifiers across all ASD datasets.

In summary, our findings for RQ1 and RQ2 indicate that tabular classifiers achieve an mean accuracy of approximately 60%. Despite efforts to enhance performance by incorporating higher-order information, such as local clustering coefficients, we did not observe significant improvements. This raises the question of whether there is a fundamental reason behind this phenomenon. We investigate this question through the concept of similarity measures.

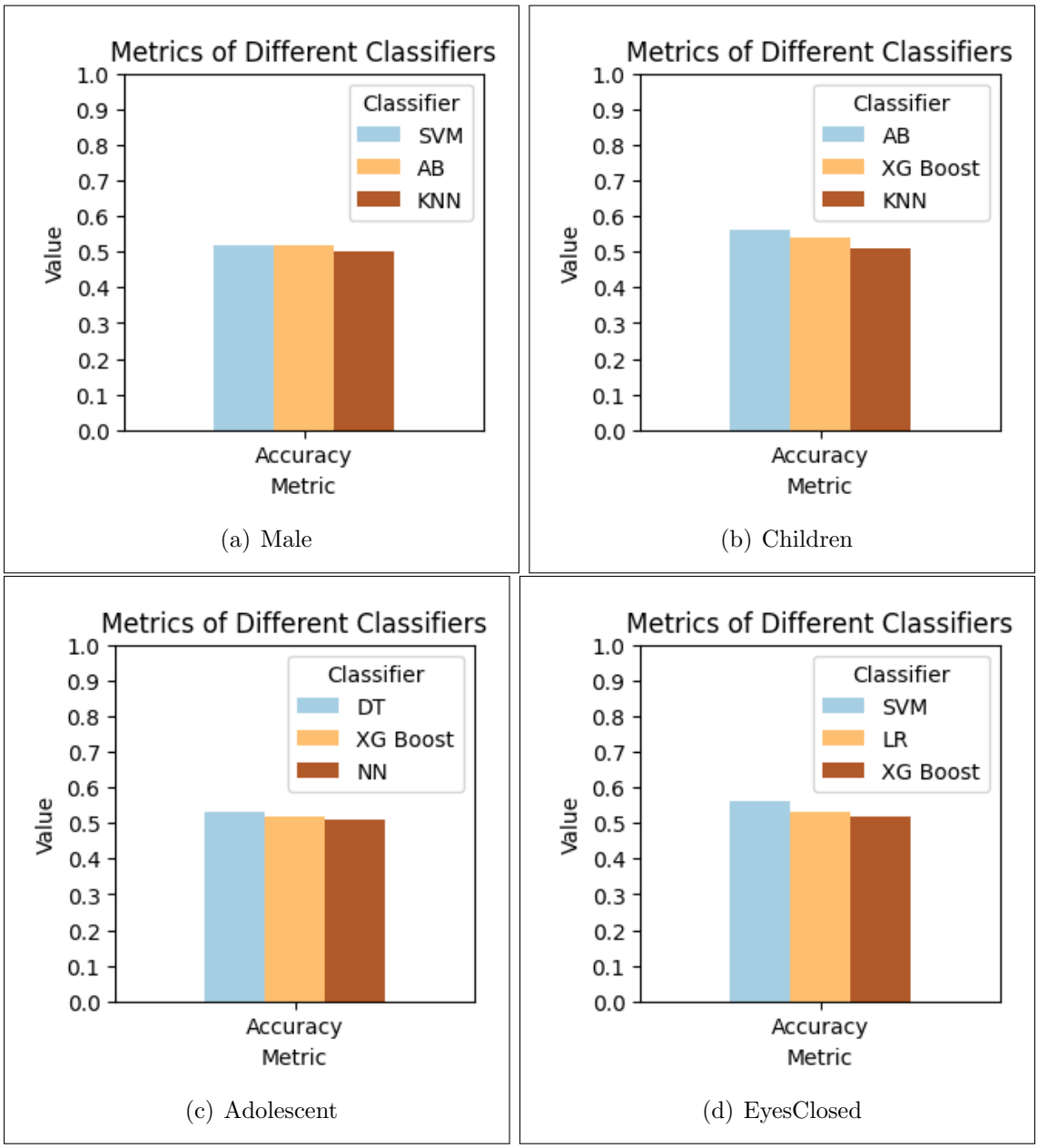

(a) Male (b) Children

(c) Adolescent (d) EyesClosed

Figure 4.3: RQ2 - Performance Metrics of Top-3 Classfiers for Top5 Node

RQ3: Can we provide evidence showing that the two classes of networks (ASD and TD) are quite similar?

The primary objective of this study is to develop improved classification models for distinguishing between typically developing (TD) and Autism Spectrum Disorder (ASD) datasets. The results obtained from Research Questions RQ1 and RQ2 have prompted further investigation into potential similarities or differences within the

Dataset	**Class(Accuracy)**		
Male	SVM(0.60)	AB(0.59)	NB(0.57)
Children	AB(0.56)	XG Boost(0.54)	KNN(0.52)
Adolescent	LR(0.59)	Pc(0.58)	SVM(0.58)
Eyesclosed	SVM(0.62)	LR(0.60)	Pc(0.58)

Table 4.4: RQ2 - Augmented Table for ASD Dataset

dataset. To verify this hypothesis, we aim to assess the presence of commonalities between ASD and TD networks. The initial approach, Hamming distance, is primarily concerned with assessing similarity based on edges within the networks and the second approach, Jaccard similarity, places its emphasis on evaluating similarity based on the vertices (nodes) present in the networks [26, 39].

Similarity based on Hamming distance.

In our first approach, we assess the similarity between the two categories of brain networks (TD and ASD) using the Hamming distance metric. When dealing with binary graphs representing structural or functional connectivity, Hamming distance is a straightforward choice for assessing network similarity or dissimilarity. It can be integrated into machine learning algorithms for classification tasks. It serves as a feature or similarity metric to differentiate between groups (e.g., healthy controls and patients with a neurological disorder) based on brain network connectivity patterns. We utilize the datasets from RQ1, where each brain network is represented as a binary string consisting of 6670 bits. Each bit in the string corresponds to a potential edge in the network, with its value indicating whether that edge is present (1) or absent (0). The Hamming distance between two brain networks is computed as the minimum number of edge flips needed to transform one network into the other, as defined in Section 3.4. The algorithm for calculating the Hamming distance is given below.

For each of the four datasets, we do the following (See Algorithm 1): For each brain network G_i in the dataset D containing ASD and TD files, we compute its Hamming distance to every other brain network G_j, $i \neq j$, in D.

Using this information, we identify the brain network G_k that is closest to G_i in terms of Hamming distance (Lines 3 to 5 of Algorithm 1). That is, the brain network G_k requires the fewest number of edge additions and deletions to convert to G_i. G_i is a *good file* if G_k is in the same class as G_i and *bad file* if G_k is not in the same class as G_i (Lines 6 to 10).

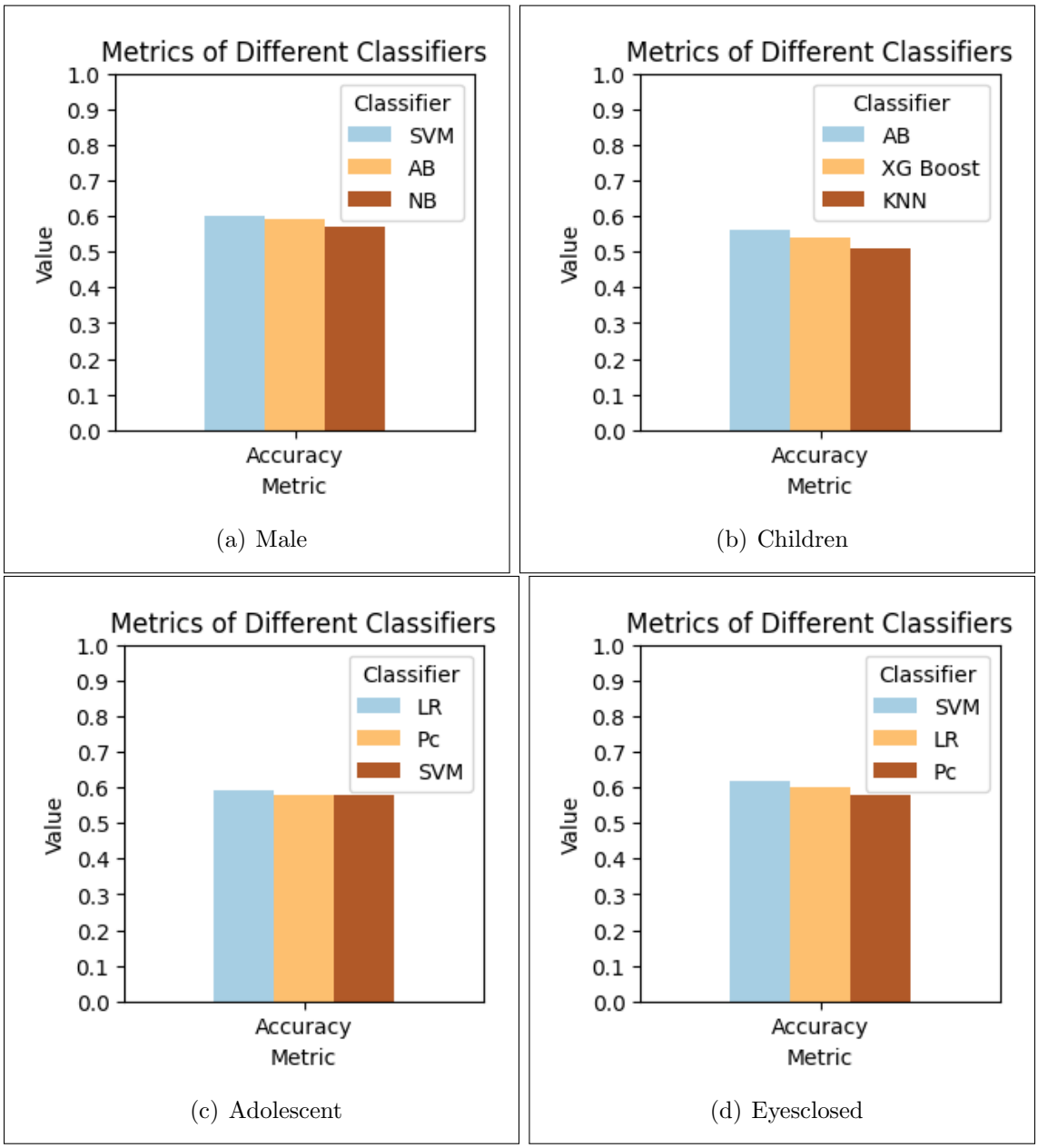

(a) Male (b) Children

(c) Adolescent (d) Eyesclosed

Figure 4.4: RQ2 - Performance Metrics of Top-3 Classfiers for Augmented Table

As results are shown in Figure 4.5, in the Adolescent dataset, we observed that both the ASD and TD classes have approximately 40% of good files (in green), indicating that around 60% are bad files (in red). This finding carries substantial significance as it highlights that, in the case of the majority of brain networks, the most closely related network belongs to the opposite category rather than its own. The consistent findings across the other three datasets (Children, Eyes Closed, Male)

Algorithm 1 Similarity based on Hamming distance

Input: A Dataset $D = \{G_1, G_2, \ldots, G_m\}$ consisting of two classes, ASD and TD files
Output: f_{ASD} and f_{TD} (the fraction of good ASD and TD files based on Hamming distance)
for each $G_i \in D$ **do**
  $class \leftarrow class(G_i)$
  $k \leftarrow \arg\min_{i \neq j} HD(G_i, G_j)$
  if G_k is in the same class as G_i **then**
    $count_{class}$++; $good_{class}$++
  else
    $count_{class}$++
  end if
end for
return $good_{ASD}/count_{ASD}$ and $good_{TD}/count_{TD}$

further solidify the conclusion that the commonly employed similarity measure falls short in effectively distinguishing between these two classes.

Dataset	**Good(TD)**	**Bad(TD)**	**Good(ASD)**	**Bad(ASD)**
Adolescent	38.46	61.54	42.86	57.14
Children	25.62	74.38	39.65	60.34
Eyes closed	44.94	55.06	56.0	44.007
Male	39.0	61.0	46.67	53.33

Table 4.5: RQ3 - Hamming Distance Results

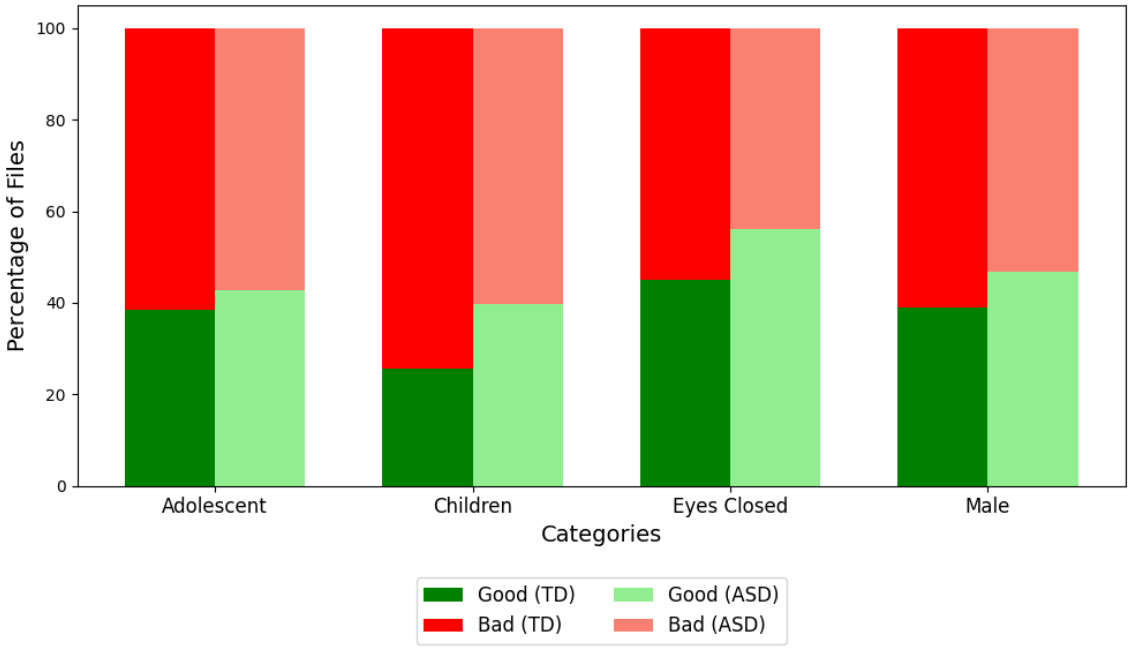

Figure 4.5: ASD Dataset: % of good and bad files using Hamming Distance

Jaccard Similarity based on k-cores.

Our approach involves employing the k-core as a "glocal" similarity measure, which combines aspects of both local and global metrics. This approach overcomes limitations found in traditional local (e.g., Hamming distance) and global (e.g., random walk-based) measures. Notably, prior research has recognized the importance of such glocal similarity measures, as discussed in [26, 39].

More specifically, we use the max-core of a brain network, as described in Section 3.4. The primary objective is to assess whether the max-core of a given brain network resembles that of a typical ASD network or a TD network, using the Jaccard similarity metric. The utilization of the k-core algorithm in brain network analysis offers several advantages and insights, making it a valuable tool in the field of neuroimaging and network neuroscience. As it allows to compare k-cores across different brain networks, such as comparing typical and atypical (e.g., ASD) networks. The k-core algorithm helps in identifying core structures within a brain network. In the context of neuroscience, these core structures can represent regions or nodes in the brain that are densely interconnected and play pivotal roles in information processing. The k-core decomposition can reveal regions with functional significance. For

example, high k-core regions may correspond to brain regions associated with critical cognitive functions or behaviors. Differences in k-core structures between healthy and disordered brains can highlight areas of dysfunction. It can aid in network visualization by highlighting the most essential and interconnected regions, making it easier to interpret complex brain network data. As, the k-core algorithm is a versatile tool for characterizing brain network structures, detecting hubs, and assessing network resilience. Its application can lead to a deeper understanding of the functional and structural organization of the brain in health and disease. It's important to mention that the computation of the max-core is computationally demanding in comparison to the Hamming distance metric.To address this computational challenge, we have devised a more efficient procedure, drawing inspiration from ideas presented in [31] (see Algorithm 2).

Algorithm 2 Jaccard similarity of Max-Core

Input: A Dataset $D = \{G_1, G_2, \ldots, G_m\}$ consisting of two classes, ASD and TD files
Output: f_{ASD} and f_{TD} (the fraction of good ASD and TD files based on Jaccard similarity of max-core)
Partition D into four sets S_{ASD}, T_{ASD}, S_{TD}, and T_{TD} using 80:20 split.
Compute SG_{ASD} and SG_{TD} using 75% threshold.
Compute their max-cores, MC_{ASD} and MC_{TD}
for each $G_i \in T_{ASD}$ **do**
    Compute max-core MC_i of G_i
    if $JS(MC_i, MC_{ASD}) > JS(MC_i, MC_{TD})$ **then**
        $count_{ASD}$++; $good_{ASD}$++
    else
        $count_{ASD}$++
    end if
end for
for each $G_i \in T_{TD}$ **do**
    Compute max-core MC_i of G_i
    if $JS(MC_i, MC_{TD}) > JS(MC_i, MC_{ASD})$ **then**
        $count_{TD}$++; $good_{TD}$++
    else
        $count_{TD}$++
    end if
end for
return $good_{ASD}/count_{ASD}$ and $good_{TD}/count_{TD}$

1. Given a dataset, we partition the ASD files in that dataset into two sets, S_{ASD} and T_{ASD} using a 80:20 split. Similarly, we partition the TD files into two sets, S_{TD} and T_{TD} using a 80:20 split (Line 3 of Algorithm 2).

2. Using the files in S_{ASD}, we create a single graph, SG_{ASD}, that we call the ASD summary graph. This graph is a graph on 116 vertices. It contains an edge (i, j) if and only if more than 75% of the graphs in S_{ASD} contain that edge. Similarly, we create the TD summary graph SG_{TD} (Line 4).

3. We compute the max cores of the two summary graphs, SG_{ASD} and SG_{TD} (Line 5).

4. Now, for each file in T_{ASD}, we compute its max-core and check if it closer to the max-core of SG_{ASD} or the max-core of SG_{TD} using Jaccard similarity. We say that it is *good* if it is closer to the max-core of SG_{ASD} and *bad* otherwise. Compute the percentage of good ASD files (Lines 6-12).

5. Repeat the previous step for TD files (Lines 13-19).

Figure 4.6 illustrates the results of our approach, representing mean percentages over ten runs. Taking the Adolescent dataset as an example, we observed that both the ASD and TD classes have approximately 40% and 60% of good files (displayed in green), respectively. This implies that the percentage of bad files is approximately 60% and 40% for ASD and TD, respectively. The noteworthy aspect of this observation is that for nearly half of the brain networks, the most similar network based on max-core comes from the opposite class, not its own. We found similar results for the other three datasets as well. This finding suggests that the Jaccard similarity of max-cores fails to differentiate between the two classes effectively.

Dataset	**Good(TD)**	**Bad(TD)**	**Good(ASD)**	**Bad(ASD)**
Adolescent	38.3285	61.6715	61.305	38.695
Children	42.723	57.277	52	48
Eyes closed	37.187	62.813	70.711	29.289
Male	39.508	60.492	58.8067	41.1933

Table 4.6: RQ3 - Jaccard Similarity Results

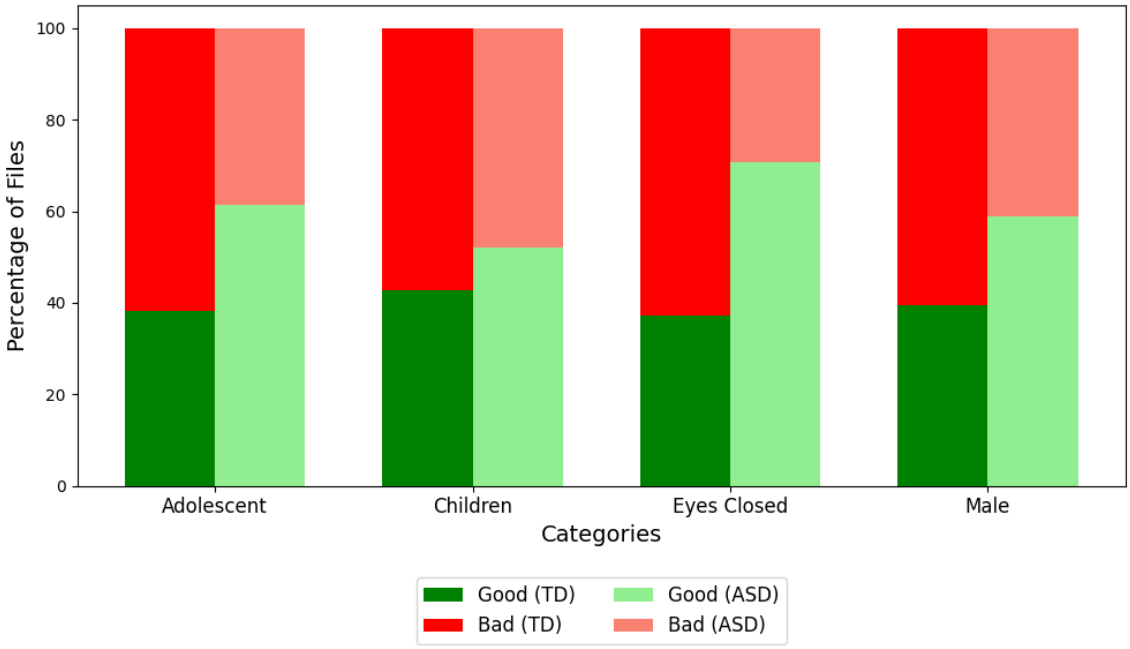

Figure 4.6: ASD Dataset: % of good and bad files using Jaccard Similarity

To summarize, the results obtained using the two approaches in RQ3 provide robust and persuasive evidence of a high degree of similarity between the graphs in the two categories: ASD and TD. There is a degree of overlap in brain network connectivity between TD individuals and those with ASD. Moreover, some individuals with ASD have brain network patterns that are more similar to TD individuals, while others may show more distinct patterns. This observed variation in results could be the potential attribute to a range of factors including research techniques and methodologies used in specific studies, specific brain regions, connectivity patterns, and the characteristics of the individuals being studied poses a challenge when trying to build classification models or use graph analysis techniques to differentiate between them in network graphs. This explains the insights of significant challenge during classification methods and graph theoretic techniques used in prior research endeavors(e.g., contrast subgraph or discriminative edges method) in achieving strong performance metrics.

Run-time. All experiments were run on a Windows machine with Intel i5 CPU and 8 GB RAM. We report here the run times for RQ1 for the larger dataset(Male) is 4 minutes and on the smallest (Children), it took 1 minute. The run times for RQ2 for the larger dataset(Male) is 6 minutes and on the smallest (Children), it took 1 minute. The run times of our algorithms for RQ3 on the largest dataset (Male), a run of Algorithm 1 took 110 minutes to finish and on the smallest (Children), it took 75 seconds. This is because Algorithm 1 computes the Hamming distance between every pair of brain networks in the dataset. Algorithm 2 was much faster and required only 92 seconds on the Male dataset and 16 seconds on the Children dataset for one run as it only compared the max-core of 20% of the networks with the two summaries computed from the rest.

4.2 Insights on ADHD Dataset

Our results for RQ1, RQ2 & RQ3 prompt the question of whether these outcomes are specific to the ASD dataset we studied. We are interested in understanding whether our approach could yield different results when applied to a dataset focused on a different but closely related health condition. To address this, we conduct an investigation using the ADHD dataset and apply the same methodology as described for the ASD dataet. ASD and ADHD are distinct neurodevelopmental disorders, but they can co-occur in individuals, with estimates suggesting that 30% to 80% of individuals with ASD may also have ADHD. Both disorders share some common symptoms such as attention difficulties, impulsivity, and hyperactivity. However, ASD is characterized by challenges in social communication and restricted/repetitive behaviors, while ADHD primarily involves symptoms related to inattention, hyperactivity, and impulsivity In our analysis for this dataset, we observed that the top three tabular classifiers achieved an accuracy rate of 63% for RQ1. Interestingly, these classifiers did not significantly outperform the baseline classifier. Furthermore, when we introduced clustering coefficients as new attributes in Research Question 2 (RQ2), we did not observe any substantial improvement in the performance metrics. as shown in Table 4.7. The accuracy for the top 5 nodes is 65%, while it is 63% for clustering coefficient, and 59% for the augmented table. In summary, incorporating higher-order information does not seem to enhance overall performance metrics.

When we compared the two classes, ADHD and TD, for RQ3, the average percentages of good files remains around 70% for Hamming distance and 43% for Jaccard

similarity, (refer to Figure 4.11). These results indicate that Hamming distance and Jaccard similarity of max-cores fails to differentiate between the two classes effectively and our findings for ASD datasets extend to the ADHD dataset as well.

Research Questions	**Class(Accuracy)**		
RQ1	Pc(0.63)	XG(0.63)	LR(0.62)
RQ2-Clustering Coeff.	XG(0.65)	Pc(0.63)	LR(0.63)
RQ2- Top5 Nodes	SVM(0.63)	NN(0.63)	NB(0.63)
RQ2-Augmented table	XG(0.59)	AB(0.59)	NB(0.59)

Table 4.7: ADHD Dataset: Accuracy for RQ1 & RQ2

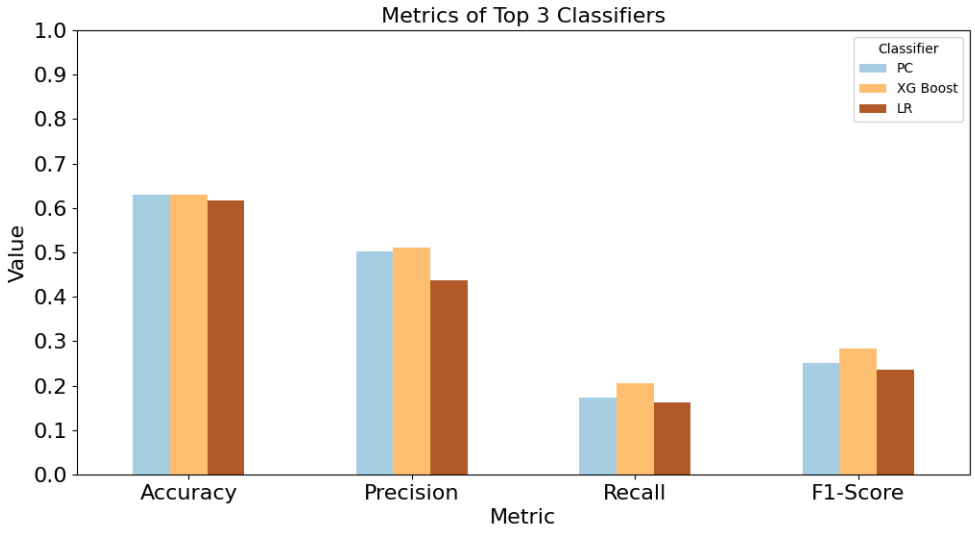

Figure 4.7: RQ1- Chart with Top-3 tabular Classifiers: ADHD dataset

Research Question 3	**Good(TD)**	**Bad(TD)**	**Good(ADHD)**	**Bad(ADHD**
Hamming Distance	70	30	31.5789	68.4211
Jaccard Similarity	42.268	57.732	59.4704	40.5296

Table 4.8: RQ3 Result

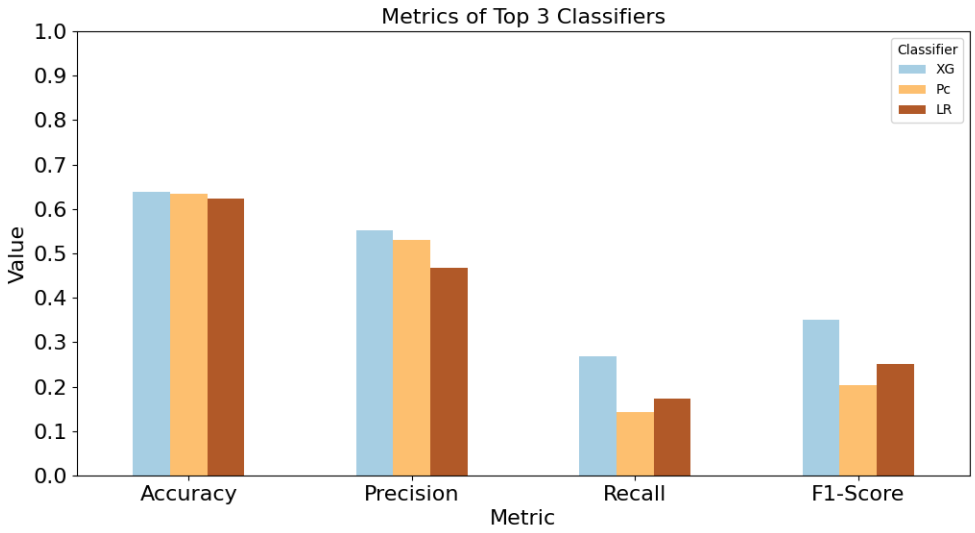

Figure 4.8: RQ2–Clustering Coeff. Chart with Top-3 Classifiers: ADHD Dataset

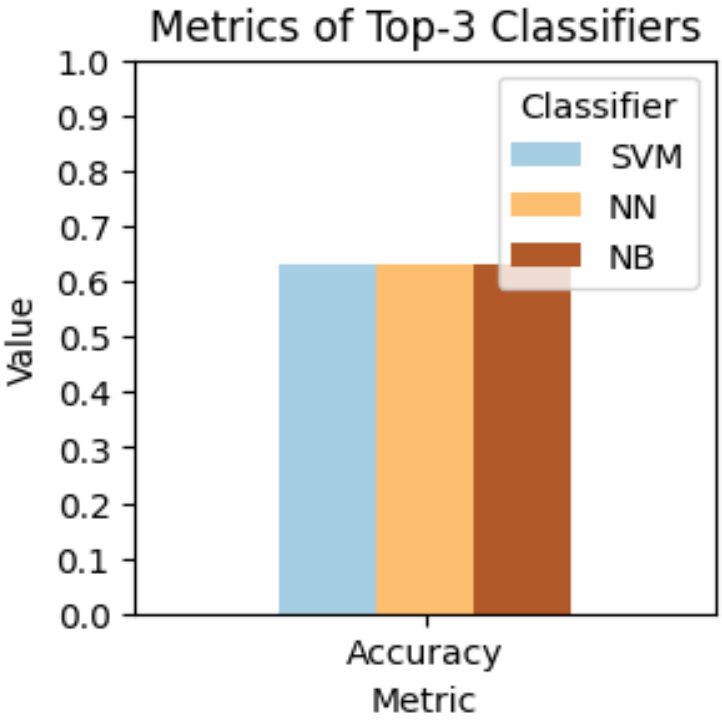

Figure 4.9: RQ2-Top5 Nodes Chart with Top-3 Classifiers: ADHD Dataset

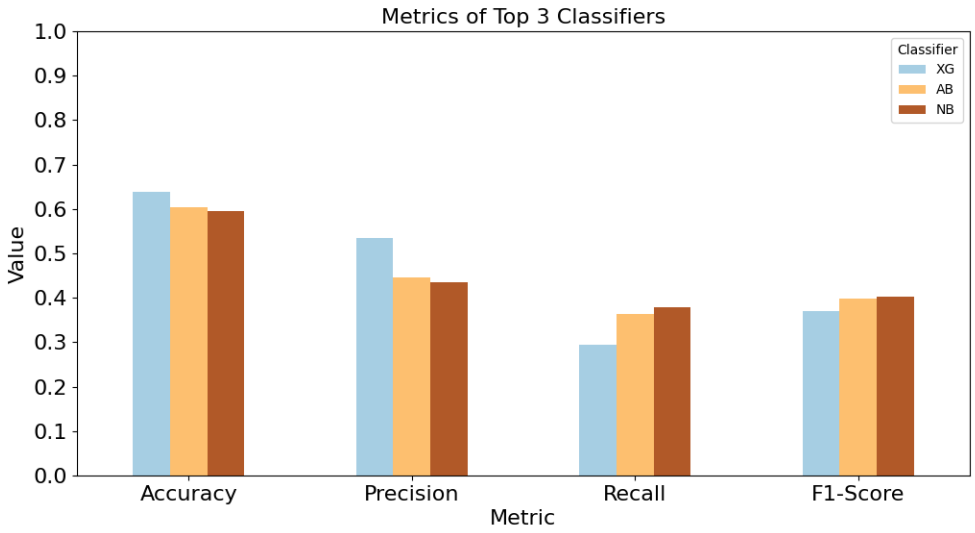

Figure 4.10: RQ2-Argumented Chart with Top-3 Classifiers:ADHD Dataset

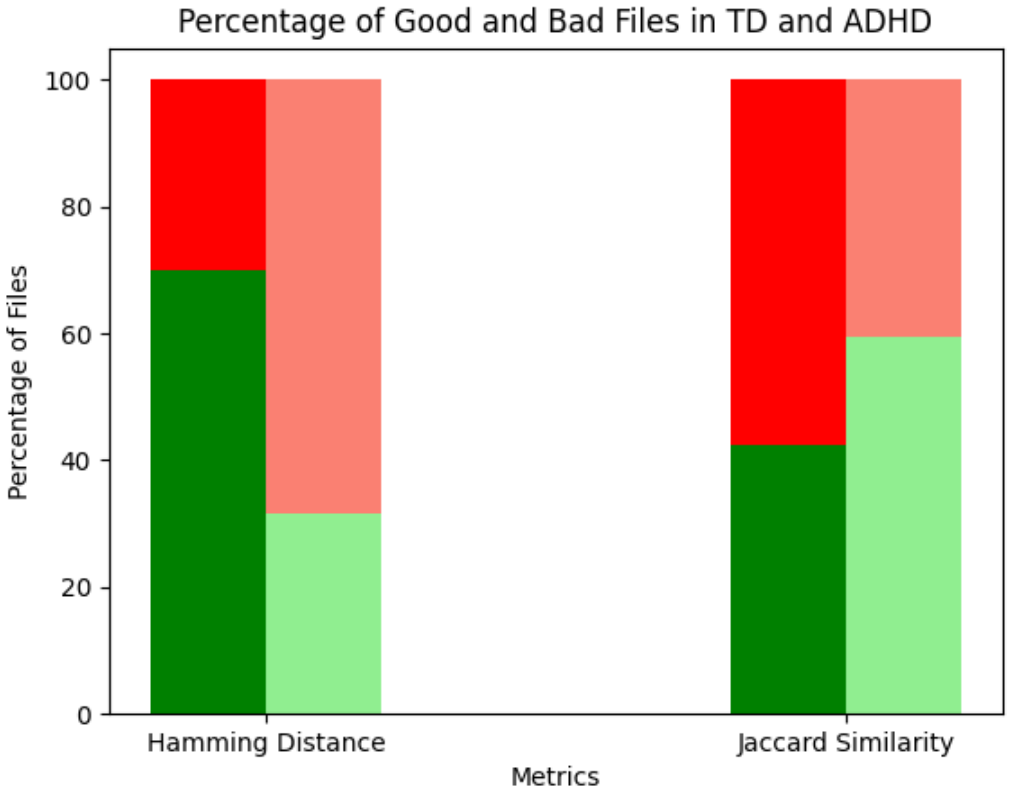

Figure 4.11: ADHD Dataset: % of good and bad files using Hamming Distance & Jaccard Similarity

Chapter 5

Conclusions

Autism is classified as a spectrum disorder due to its inclusion of a broad spectrum of symptoms and varying degrees of impairment, spanning from mild to severe. Early diagnosis and appropriate interventions like medical services and social support can significantly improve the quality of life for individuals with ASD or other related developmental disorders. Considering the limited knowledge and information of the causes and absence of a cure, it is imperative to explore novel techniques to enhance the diagnosis of this condition.

This work investigates the potential of biomarkers obtained from fMRI scans in the diagnosis of ASD and ADHD. This indicates that tabular classifiers can achieve performance levels comparable to the most established graph-theoretic methods while maintaining interpretability. Simultaneously, this highlights the difficulties associated with classifying brain networks when utilizing two similarity metrics: the Hamming distance and the Jaccard similarity of max-cores, especially when applied to existing datasets. Incorporating higher-order connectivity patterns, such as triangles, local clustering coefficients did not improved the classification accuracy. These challenges could potentially hinder the accuracy and reliability of the classification process. Further research is required to understand the reasons behind these difficulties and to develop improved approaches for brain network classification.

One promising avenue to address the current challenges lies in the use of larger fMRI datasets. By expanding the dataset size, researchers can potentially mitigate some of the issues encountered in the current study. A larger dataset would provide a more comprehensive representation of brain patterns and improve the generalizability of the findings. The result highlights the surprising efficacy of tabular classifiers compared to more complex graph-theoretic methods, which can facilitate better diagnostic

tools. Nevertheless, challenges related to brain network classification using specific similarity measures emphasize the need for further investigation and advancements. By utilizing larger fMRI datasets, researchers can overcome current limitations and pave the way for significant progress in understanding and diagnosing these developmental disorders and thus leading to further progress. Another possible avenue is to explore the use of four-node graphlets as higher-order information to improve accuracy [44]. The hope is that the discoveries and recommendations from this study will prove beneficial in guiding future endeavors towards achieving this objective.

Bibliography

[1] Halim Abbas, Ford Garberson, Stuart Liu-Mayo, Eric Glover, and Dennis P Wall. Multi-modular ai approach to streamline autism diagnosis in young children. *Scientific reports*, 10(1):1–8, 2020.

[2] Carlo Abrate and Francesco Bonchi. Counterfactual graphs for explainable classification of brain networks. In *KDD*, pages 2495–2504, 2021.

[3] Steward Mostofsky Adirana Di Martino. Abide. `http://fcon_1000.projects.nitrc.org/indi/abide/abide_I.html`.

[4] APA. *Diagnostic and statistical manual of mental disorders : DSM-5™*. American Psychiatric Publishing, a division of American Psychiatric Association, Washington, DC ;, 5th edition. edition, 2013.

[5] Mohammad R. Arbabshirani, Sergey Plis, Jing Sui, and Vince D. Calhoun. Single subject prediction of brain disorders in neuroimaging: Promises and pitfalls. *NeuroImage (Orlando, Fla.)*, 145(Pt B):137–165, 2017.

[6] Onur Asan, Alparslan Emrah Bayrak, and Avishek Choudhury. Artificial intelligence and human trust in healthcare: Focus on clinicians. *J Med Internet Res*, 22(6):e15154, Jun 2020.

[7] Maksymilian A. Brzezicki, Nicholas E. Bridger, Matthew D. Kobetić, Maciej Ostrowski, Waldemar Grabowski, Simran S. Gill, and Sandra Neumann. Artificial intelligence outperforms human students in conducting neurosurgical audits. *Clinical Neurology and Neurosurgery*, 192:105732, 2020.

[8] Ed Bullmore and Olaf Sporns. Complex brain networks: graph theoretical analysis of structural and functional systems. *Nature reviews neuroscience*, 10(3):186–198, 2009.

[9] CDC. Cdc. https://www.cdc.gov/ncbddd/autism/data.html.

[10] Corinna Coupette, Sebastian Dalleiger, and Jilles Vreeken. Differentially describing groups of graphs. *Proc. of AAAI Conference on Artificial Intelligence*, 36(4):3959–3967, Jun. 2022.

[11] Luis de la Torre-Ubieta, Hyejung Won, Jason L Stein, and Daniel H Geschwind. Advancing the understanding of autism disease mechanisms through genetics. *Nature medicine*, 22(4):345–361, 2016.

[12] A Di Martino, C-G Yan, Q Li, E Denio, F X Castellanos, K Alaerts, J S Anderson, M Assaf, S Y Bookheimer, M Dapretto, B Deen, S Delmonte, I Dinstein, B Ertl-Wagner, D A Fair, L Gallagher, D P Kennedy, C L Keown, C Keysers, J E Lainhart, C Lord, B Luna, V Menon, N J Minshew, C S Monk, S Mueller, R-A Müller, M B Nebel, J T Nigg, K O'Hearn, K A Pelphrey, S J Peltier, J D Rudie, S Sunaert, Mark Thioux, J M Tyszka, L Q Uddin, J S Verhoeven, N Wenderoth, J L Wiggins, S H Mostofsky, and M P Milham. The autism brain imaging data exchange: towards a large-scale evaluation of the intrinsic brain architecture in autism. *Molecular psychiatry*, 19(6):659–67, 2014.

[13] Charles Elkan. Evaluating classifiers. *UC San Diego*, 2012.

[14] Keanelek Enns, Venkatesh Srinivasan, and Alex Thomo. Identifying autism spectrum disorder using brain networks: Challenges and insights. *Proc. of Int. Conf. on Information, Intelligence, Systems and Applications (IISA)*, 2023.

[15] Peter G Enticott, Hayley A Kennedy, Nicole J Rinehart, Bruce J Tonge, John L Bradshaw, John R Taffe, Zafiris J Daskalakis, and Paul B Fitzgerald. Mirror neuron activity associated with social impairments but not age in autism spectrum disorder. *Biological psychiatry*, 71(5):427–433, 2012.

[16] Gerald Fischbach. Leo kanner's 1943 paper on autism. https://www.spectrumnews.org/opinion/viewpoint/leo-kanners-1943-paper-on-autism/.

[17] Alexander L Fogel and Joseph C Kvedar. Artificial intelligence powers digital medicine. *NPJ digital medicine*, 1(1):1–4, 2018.

[18] World Health Organization. Regional Office for the Eastern Mediterranean. Autism spectrum disorders. Technical documents, 2019.

[19] Katja Grace, John Salvatier, Allan Dafoe, Baobao Zhang, and Owain Evans. When will ai exceed human performance? evidence from ai experts. *Journal of Artificial Intelligence Research*, 62:729–754, 2018.

[20] Xinyu Guo, Kelli C. Dominick, Ali A. Minai, Hailong Li, Craig A. Erickson, and Long J. Lu. Diagnosing autism spectrum disorder from brain resting-state functional connectivity patterns using a deep neural network with a novel feature selection method. *Frontiers in Neuroscience*, 11, 2017.

[21] Leonardo Gutiérrez-Gómez and Jean-Charles Delvenne. Unsupervised network embeddings with node identity awareness. *Applied Network Science*, 4(1):1–21, 2019.

[22] Ali Hassan, Riza Sulaiman, Mansoor Abdulgabber, and Hasan Kahtan. Towards user-centric explanations for explainable models: A review. *J. of Information System and Technology Management*, 6:36–50, 2021.

[23] Leanna M Hernandez, Jeffrey D Rudie, Shulamite A Green, Susan Bookheimer, and Mirella Dapretto. Neural signatures of autism spectrum disorders: insights into brain network dynamics. *Neuropsychopharmacology (New York, N.Y.)*, 40(1):171–189, 2015.

[24] Susan L Hyman, Susan E Levy, Scott M Myers, Dennis Z Kuo, Susan Apkon, Lynn F Davidson, Kathryn A Ellerbeck, Jessica EA Foster, Garey H Noritz, Mary O'Connor Leppert, et al. Identification, evaluation, and management of children with autism spectrum disorder. *Pediatrics*, 145(1), 2020.

[25] Tetsuya Iidaka. Resting state functional magnetic resonance imaging and neural network classified autism and control. *Cortex*, 63:55–67, 2015.

[26] Giuseppe Jurman, Roberto Visintainer, Michele Filosi, Samantha Riccadonna, and Cesare Furlanello. The him glocal metric and kernel for network comparison and classification. In *DSAA*, pages 1–10, 2015.

[27] Andrew B Kahng. Ai system outperforms humans in designing floorplans for microchips, 2021.

[28] Wissam Khaouid, Marina Barsky, Venkatesh Srinivasan, and Alex Thomo. K-core decomposition of large networks on a single pc. *PVLDB*, 9(1):13–23, 2015.

[29] Marjane Khodatars, Afshin Shoeibi, Delaram Sadeghi, Navid Ghaasemi, Mahboobeh Jafari, Parisa Moridian, Ali Khadem, Roohallah Alizadehsani, Assef Zare, Yinan Kong, Abbas Khosravi, Saeid Nahavandi, Sadiq Hussain, U. Rajendra Acharya, and Michael Berk. Deep learning for neuroimaging-based diagnosis and rehabilitation of autism spectrum disorder: A review. *Computers in biology and medicine*, 139:104949–104949, 2021.

[30] Yazhou Kong, Jianliang Gao, Yunpei Xu, Yi Pan, Jianxin Wang, and Jin Liu. Classification of autism spectrum disorder by combining brain connectivity and deep neural network classifier. *Neurocomputing*, 324:63–68, 2019.

[31] Tommaso Lanciano, Francesco Bonchi, and Aristides Gionis. Explainable classification of brain networks via contrast subgraphs. In *KDD*, pages 3308–3318, 2020.

[32] Marlene Briciet Lauritsen. Autism spectrum disorders. *European child & adolescent psychiatry*, 22:37–42, 2013.

[33] Pantelis Linardatos, Vasilis Papastefanopoulos, and Sotiris Kotsiantis. Explainable ai: A review of machine learning interpretability methods. *Entropy*, 23(1), 2021.

[34] Yaya Liu, Lingyu Xu, Jun Li, Jie Yu, and Xuan Yu. Attentional connectivity-based prediction of autism using heterogeneous rs-fmri data from cc200 atlas. *Experimental neurobiology*, 29(1):27–37, 2020.

[35] Jose O. Maximo, Elyse J. Cadena, and Rajesh K. Kana. The implications of brain connectivity in the neuropsychology of autism. *Neuropsychology review*, 24(1):16–31, 2014.

[36] Muhammad Faiz Misman, Azurah A Samah, Farah Aqilah Ezudin, Hairuddin Abu Majid, Zuraini Ali Shah, Haslina Hashim, and Muhamad Harun. Classification of adults with autism spectrum disorder using deep neural network. In *AiDAS'19*, pages 29–34.

[37] Sharmila Banerjee Mukherjee. Autism spectrum disorders—diagnosis and management. *The Indian Journal of Pediatrics*, 84:307–314, 2017.

[38] NHS. Nhs. `https://www.nhs.uk/conditions/attention-deficit-hyperactivity-disorder-adhd/`.

[39] Giannis Nikolentzos, Polykarpos Meladianos, Stratis Limnios, and Michalis Vazirgiannis. A degeneracy framework for graph similarity. In *IJCAI*, pages 2595–2601, 2018.

[40] Hidir Selcuk Nogay and Hojjat Adeli. Machine learning (ml) for the diagnosis of autism spectrum disorder (asd) using brain imaging. *Reviews in the neurosciences*, 31(8):825–841, 2020.

[41] Alan Perotti, Paolo Bajardi, Francesco Bonchi, and André Panisson. Graphshap: Motif-based explanations for black-box graph classifiers. *arXiv preprint arXiv:2202.08815*, 2022.

[42] Nataša Pržulj. Biological network comparison using graphlet degree distribution. *Bioinformatics*, 23(2):e177–e183, 2007.

[43] Caio Pinheiro Santana, Emerson Assis de Carvalho, Igor Duarte Rodrigues, Guilherme Sousa Bastos, Adler Diniz de Souza, and Lucelmo Lacerda de Brito. rs-fmri and machine learning for asd diagnosis: a systematic review and meta-analysis. *Scientific reports*, 12(1):6030–6030, 2022.

[44] Yudi Santoso, Venkatesh Srinivasan, and Alex Thomo. Efficient enumeration of four node graphlets at trillion-scale. In *EDBT*, pages 439–442, 2020.

[45] Pascal Shervashidze, Nino andf Schweitzer, Erik Jan Van Leeuwen, Kurt Mehlhorn, and Karsten M Borgwardt. Weisfeiler-lehman graph kernels. *Journal of Machine Learning Research*, 12(9), 2011.

[46] Faria Zarin Subah, Kaushik Deb, Pranab Kumar Dhar, and Takeshi Koshiba. A deep learning approach to predict autism spectrum disorder using multisite resting-state fmri. *Applied Sciences*, 11(8), 2021.

[47] Rajat Mani Thomas, Selene Gallo, Leonardo Cerliani, Paul Zhutovsky, Ahmed El-Gazzar, and Guido van Wingen. Classifying autism spectrum disorder using the temporal statistics of resting-state functional mri data with 3d convolutional neural networks. *Frontiers in Psychiatry*, 11, 2020.

[48] Sana Tonekaboni, Shalmali Joshi, Melissa D McCradden, and Anna Goldenberg. What clinicians want: contextualizing explainable machine learning for clinical end use. In *Machine learning for healthcare conference*, pages 359–380. PMLR, 2019.

[49] Hao Wang, Yue Deng, Linyuan Lü, and Guanrong Chen. Hyperparameter-free and explainable whole graph embedding. *CoRR*, abs/2108.02113, 2021.

[50] Choong-Wan Woo, Luke J Chang, Martin A Lindquist, and Tor D Wager. Building better biomarkers: brain models in translational neuroimaging. *Nature neuroscience*, 20(3):365–377, 2017.

[51] Guang Yang, Qinghao Ye, and Jun Xia. Unbox the black-box for the medical explainable ai via multi-modal and multi-centre data fusion: A mini-review, two showcases and beyond. *Information Fusion*, 77:29–52, 2022.

Appendix A

Reproducibility

Repositories:

- This study: `https://github.com/Tabassum61/HIBIBI2023`
- "Explainable Classification of Brain Networks via Contrast Subgraphs": `https://github.com/tlancian/contrast-subgraph`